A&A 376, 917–927 (2001)
DOI: 10.1051/0004-6361:20010947

Astronomy & Astrophysics

The η Carinae spectrum of SS73 11 (=Ve 2-27)⋆

S. J. C. Landaberry, C. B. Pereira, and F. X. de Araújo

Observatório Nacional-MCT, Rua José Cristino, 77, CEP 20921-400, São Cristóvão, Rio de Janeiro-RJ, Brazil

Received 20 March 2001 / Accepted 14 June 2001

Abstract. We report new spectroscopic observations of the peculiar emission-line star SS73 11, between 3200 Å and 7200 Å. A line list is provided with their suggested identifications. From the measurements of several forbidden and permitted emission lines of single ionized iron, we derived the color excess and the excitation temperature. We also discuss the nature of SS73 11 based on data obtained. The spectrum closely resembles not only η Car but also some proto-planetary nebulae. On the other hand we concluded that this object is not a B[e]-supergiant, a symbiotic star or a Herbig AeB[e]-star.

Key words. stars: emission-line, Be – stars: AGB and post-AGB – stars: individual: η Car

1. Introduction

SS73 11 was discovered as a emission-line object by Velghe (1957). In his paper, he reported SS73 11 (Ve 2-27) having "Hα very strong and starlike. Faint continuum distinguishable. Not visible on blue-sensitive plates". Westerlund & Henize (1967) also note the starlike appearance of SS73 11 when comparing it with some southern planetary nebulae. In the following years, several authors noted the flat continuum of SS73 11, which could be in principle evidence for a planetary nebulae-like object. However, due to the absence of lines of higher excitation such as [O III], [Ne III], this object was rejected as a planetary nebula (Webster 1966; Henize 1967; Stenholm & Acker 1987; Acker et al. 1987). In the ESO Catalogue of Planetary Nebulae it is classified as peculiar emission-line source (Acker et al. 1992).

SS73 11 was also recognized as an emission object in the objective prism survey of Sanduleak & Stephenson (1973). In that paper the authors classify it as a doubtful very-low-excitation object. The first spectral classification was given by Allen & Swings (1976). They classified it as peculiar Be star with infrared excess after having selected this star from previous photometric surveys done in the infrared (Allen & Glass 1974, 1975).

As part of a long-term program to investigate emission-line objects in the southern hemisphere, we recently started a spectroscopic survey at the European Southern Observatory (ESO) of some stars from Sanduleak & Stephenson (1973) sample. This survey is also part of a program to study emission-line objects whose nature is not well established in the literature. In this paper we analyze the peculiar emission-line object SS73 11. In Sect. 2 we present the data, including the observations and the reduction procedure, extinction and the spectra. In Sect. 3 we present the physical conditions of the object, the excitation temperature using iron emission lines and the electron density and temperature. We also used the Self Absorption Curve (SAC) method (Friedjung & Muratorio 1987) to analyze the physical conditions of the iron-emitting region. In Sect. 4 we discuss the nature of SS73 11 and the conclusions are given in the last section.

2. The data

2.1. Observations and reduction

Spectroscopic observations were performed using a Boller & Chivens spectrograph at the Cassegrain focus of the ESO 1.52 m telescope in La Silla (Chile) at January 19, 1998, March 2 and 4 and December 18, 1999. A UV-flooded thinned Loral Lesser CCD #39 (2048 × 2048, 15 μm/pixel) was used as the detector; it gives a high quantum efficiency in the blue and in the UV. The setup employed is the same as that used to investigate other emission-line objects with the 1.52 m telescope (Pereira et al. 2001). Two instrumental setups were employed. The first made use of grating #23 with 600 l/mm, providing a resolution of 4.6 Å in the range $\lambda\lambda$3500 Å–7500 Å and the other used the grating #31 with 1200 l/mm, resulting in a resolution of 1.9 Å in the range $\lambda\lambda$3100 Å–5100 Å.

The spectra were reduced using standard IRAF tasks, from bias subtraction and flat-field correction, through

Send offprint requests to: S. J. C. Landaberry,
e-mail: sayd@on.br

⋆ Based on observations made with the 1.52 m telescope at the European Southern Observatory (La Silla, Chile) under the agreement with the Observatório Nacional, Brazil.

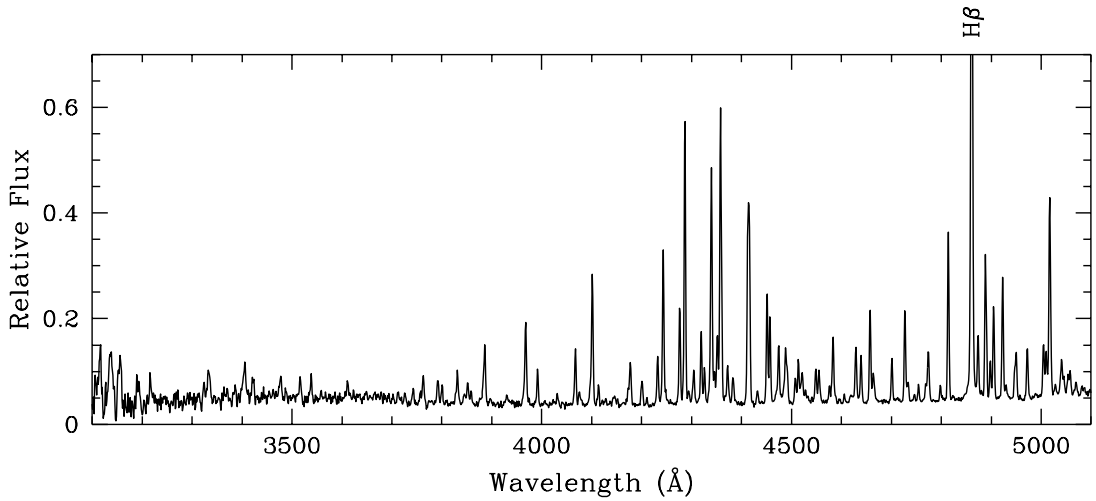

Fig. 1. Blue spectrum of SS73 11. Notice the presence of several emission lines of single ionized iron.

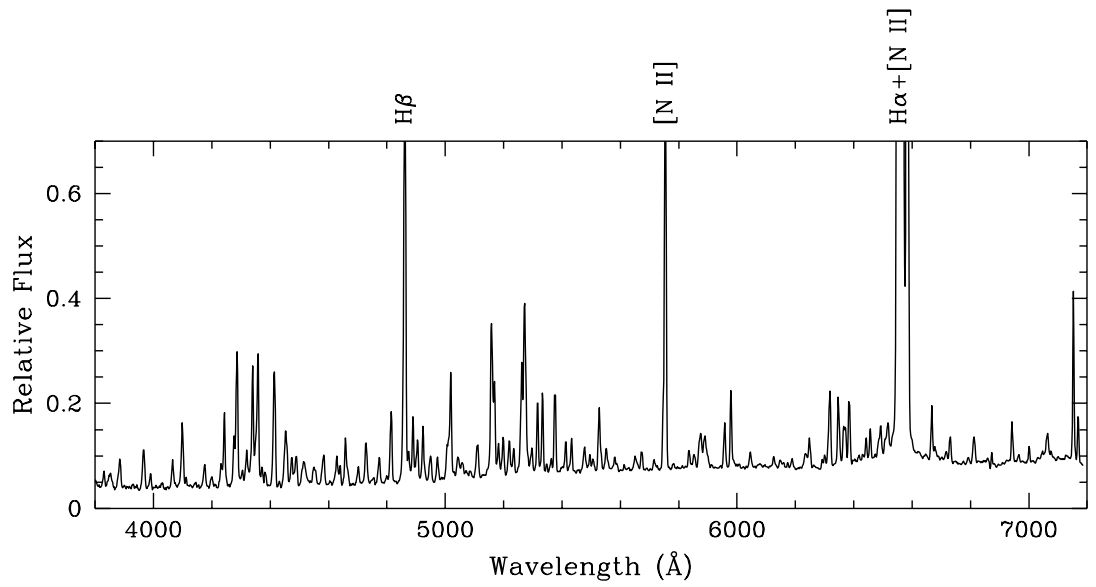

Fig. 2. Optical spectrum of SS73 11. Notice the strength of [N II] 5754 Å.

spectral extraction and wavelength and flux calibration. Spectrophotometric standards from Oke (1974) and Hamuy et al. (1994) were observed. The slit orientation in the range (3200 Å–5100 Å) was aligned with the parallactic angle in order to minimize the light loss due to atmospheric refraction.

In the linearized spectra, the fluxes of emission lines have been measured by the conventional method adjusting a gaussian function to the line profile thereby obtaining the intensity, the central wavelength and the line width at half power level. Uncertainties in the line intensities come mainly from the position of the underlying continuum. We estimate the errors in the fluxes to be about 20% for weaker lines (line fluxes ≈10 on the scale of Hβ = 100) and about 10% for stronger lines.

We also observed SS73 11 in high resolution mode ($R \approx$ 48 000) with FEROS (Kaufer et al. 1999) with the 1.52 m ESO telescope of La Silla (Chile) on December 18, 1999 with 3300 s of exposure time. These data will be carefully analyzed in a future work. In the present paper we have used it to better identify some features that are blended in the low resolution spectra.

2.2. The spectrum of SS73 11

Our Cassegrain data of SS73 11 are displayed in Figs. 1 and 2. Figure 1 shows the spectrum in the λ 3200–5100Å, range, at a resolution of 1.9 Å and Fig. 2 shows the $\lambda 3800 - 7200$ Å range at a resolution of 4.6 Å. The spectrum is completely dominated by several strong emission lines over a flat continuum.

In order to identify the lines we used mostly the lists provided by Thackeray (1967) and Moore (1945). Table 1 presents the observed wavelength (Col. 1), the measured line intensity in units of Hβ = 100 (Col. 2), and the identification proposed by us (Col. 3). The third column gives

Table 1. Observed emission line fluxes relative to Hβ = 100.

Wavelength	$F(\lambda)$	Identification
3216.3	5.2	Cr II[6F], 16.32
3323.8	2.3	N III[6F], 23.16
3327.9	1.9	
3332.6	4.8	S III(2), 33.16
3339.8	1.6	Fe III(7), 38.36
3360.0	4.4	Fe II(105), 60.10
		Cr II(21), 60.29
3366.5	2.2	
3377.4	2.2	Fe II[26F], 76.20
		N III[5F], 78.55
3389.9	3.8	Fe II[26F], 87.10
3395.9	0.8	N III[4F], 93.2
3405.5	5.2	
3411.9	1.0	
3427.0	5.0	
3442.0	1.9	Fe II[26F], 40.99
3515.6	4.3	
3527.6	2.1	Cr II(109), 28.23
3537.9	4.0	Fe II[26F], 38.69-39.19
3541.6	0.9	
3550.3	2.1	N II(5), 51.534
3612.0	2.1	Cr II(13), 13.26
		Fe II(112), 14.873
		HeI(6), 13.64
3618.1	2.9	Cr II(147), 17.32
3742.2	2.9	Fe II(15), 41.56
3756.9	2.0	Cr II(144), 56.55
3763.0	4.1	Fe II(29), 64.09
3800.2	2.5	H 10
		Fe III(47), 00.43
3831.2	4.0	H 9
3845.5	1.6	Fe II[8F], 47.78
3852.4	2.7	Fe II[9F], 51.63
		S III(1), 53.657
3859.2	1.4	
3885.9	7.3	H 8
		HeI, 88.65
3930.7	1.6	Fe II(3), 30.31
3968.0	10.2	Fe II(3), 69.38+69.40
		Fe II[8F], 68.27
		Fe II[24F], 68.66
		Hϵ
3974.6	0.6	Fe II(29), 74.16
3991.4	3.5	Cr II[4F], 92.08+93.57
		N III[4F], 93.65
4031.6	1.5	Fe II(126), 32.95
		N III[4F], 33.1
4067.4	6.1	N III(11), 67.05
		S II[1F], 68.62
4075.7	1.9	S II[1F], 76.22
4100.4	15.2	Hδ
4113.1	2.2	Fe II[23F], 14.48
4172.9	2.5	Fe II(27), 73.45
4177.3	4.6	Fe II[21F], 77.21
		Fe II(28), 78.86
4199.6	2.9	Fe II(141), 99.09
		He II(3), 99.83
4232.1	5.6	Fe II[21F], 31.56
		Fe II(27), 33.167
4243.3	15.9	Fe II[21F], 43.98+44.81
4248.4	1.3	Fe II[36F], 49.07
		N III[4F], 49.48
4276.0	10.1	Fe II[21F], 76.83
4286.6	28.9	Fe II[7F], 87.40
4305.1	3.8	Fe II[21F], 05.90
4319.4	7.8	Fe II[21F], 19.62
4326.0	3.7	N III[3F], 26.85
4340.2	27.4	Hγ
4346.4	3.3	Fe II[21F], 46.85
		Fe II[36F], 47.35
4352.4	8.6	Fe II[21F], 52.78
		Fe II(27), 51.76
4358.9	31.4	Fe II[6F], 58.10
		Fe II[7F], 59.34
		Fe II[21F], 58.37
4372.3	4.6	Fe II[21F], 72.43
4383.2	3.3	Fe II[6F], 82.75
4385.6	1.8	Fe II(27), 85.38
4414.1	14.3	Fe II[7F], 13.78
	17.1	Fe II[6F], 16.27
4431.8	1.7	Fe II[6F], 32.45
4451.4	11.9	Fe II[7F], 52.11
4457.2	9.2	Fe II[6F], 57.95
4475.1	8.6	Fe II[7F], 74.91
4488.8	8.8	Fe II[6F], 88.75
		Fe II(37), 89.19
4493.4	0.9	Fe II[6F], 92.60
4507.4	33.1	Fe II(38), 08.28
		Fe II[6F], 09.61
4513.9	4.9	N III(3), 14.89
		Fe II(20), 15.19
		Fe II(37), 15,34
		Fe II[6F], 14.90
4520.2	2.5	Fe II(37), 20.23
4522.2	2.7	Fe II(38), 22.64
4527.1	1.6	Fe II[6F], 28.39
4532.1	0.8	Fe II[6F], 33.00
		Fe II(37), 34.17
4540.8	0.6	Fe II(38), 41.52
4548.3	4.2	Fe II(38), 49.47
		Fe II[6F], 50.48
4554.9	4.2	Fe II(37), 55.75
4575.3	2.2	Fe II(38), 76.33
		Fe II[a2G-c2D], 76.4
4582.5	8.2	Fe II(37), 82.84
		Fe II(38), 83.83
		Fe II(26), 83.99
4607.1	0.8	N II(5), 07.15
4628.6	2.6	N III[3F], 28.1
	4.5	Fe II(37), 29.34
4639.2	5.3	Fe II[4F], 39.68
4657.7	4.8	Fe II(43), 56.97
	5.3	Fe III[3F], 58.1
4664.4	4.6	Fe II[4F], 64.45
		Fe II[5F], 64.97
		Fe II(44), 63.70
		Fe II(17), 64.79
4701.1	4.8	Fe III[3F], 01.5
4727.8	10.1	Fe II[4F], 28.07
4733.0	2.5	Fe III[3F], 33.9

Table 1. continued.

Wavelength	$F(\lambda)$	Identification
4746.0	0.9	Fe II[20F], 45.49
4754.2	1.9	Fe III[3F], 54.7
		S II(35), 55.12
4769.1	2.1	Fe III[3F], 69.4
4774.3	6.2	OI(16), 73.76
		Fe II[20F], 74.74
		N II(20), 74.222
4798.2	2.3	Fe II[4F], 98.28
4814.4	17.2	Fe III[3F], 13.9
		Fe II[20F], 14.55
4861.1	100.0	Hβ
4874.0	6.1	Fe II[20F], 74.49
4889.2	13.3	Fe II[4F], 89.63
4898.0	4.0	Fe II[a2G-b2D], 98.61
4904.8	9.9	Fe II[20F], 05.35
4923.2	13.0	Fe II(42), 23.92
4930.1	2.2	Fe III[1F], 30.5
4947.1	1.7	Fe II[20F], 47.38
4950.4	2.9	Fe II[20F], 50.74
4972.5	6.1	Fe II[20F], 73.39
4984.5	0.7	Fe III[2F], 85.9
4989.0	1.1	Fe III[2F], 87.2
5004.1	5.8	Fe II[20F], 05.52
5007.2	4.2	Fe II[4F], 06.52
5009.6	1.0	S II(7), 09.54
5011.5	2.8	Fe III[1F], 11.3
		N II(64), 11.24+12.02
5016.8	19.0	N II(19), 16.387
		Fe II(42), 18.434
		HeI(4), 15.675
5020.2	5.3	Fe II[20F], 20.24
5026.5	0.6	Ti III[11F], 25.53
5028.2	1.0	Fe II[a2G-b2D], 28.0
5041.3	1.4	S III(5), 41.063
5043.4	3.2	Fe II[20F], 43.53
5046.2	2.1	S II(15), 47.28
		Fe II[a2P-c2D], 48.18
5053.7	1.9	S III(5), 56.020+56.35
5057.9	2.6	Fe II[a2G-b2D], 60.08
5070.0	2.1	Fe II[19F], 72.40
5081.2	1.0	Fe II[35F], 83.72
5086.5	1.7	Fe II[3], 86.52
5107.7	3.1	Fe II[18F], 07.95
5110.4	6.2	Fe III[1F], 11.30
		Fe II[19F], 11.63
5158.8	24.1	Fe II[18F], 58.00
		Fe II[19F], 58.81
5162.5	9.2	Fe II[35F], 63.94
5168.7	19.9	Fe II(42), 69.03
5182.1	6.4	Fe II[18F], 81.97
		MgI(2), 83.60
		Fe II[19F], 84.80
5198.1	4.3	Fe II(49), 97.569
	3.7	Fe II[35F], 99.18
5219.8	6.4	Fe II[19F], 20.06
5234.8	5.3	Fe II(49), 34.62
5261.5	22.8	Fe II[19F], 61.61
5268.6	6.2	Fe II[18F], 68.88
5270.2	6.1	Fe III[1F], 70.4
5272.1	30.3	Fe II[18F], 73.38

Wavelength	$F(\lambda)$	Identification
5276.0	5.8	Fe II(49), 75.99
5278.5	0.8	SI(4), 78.10+78.70
5283.3	2.3	Fe II[35F], 83.10
5291.6	0.8	Fe III, 91.78
5296.7	4.8	Fe II[17F], 95.70
		Fe II[19F], 96.84
5306.3	0.4	Cr II(24), 05.85
5316.2	13.8	Fe II(49), 16.61
		Fe II(48), 16.78
5333.2	14.4	Fe II[19F], 33.65
5346.9	1.2	Fe II[18F], 47.67
5362.9	2.4	Fe II(48), 62.86
5375.7	15.4	Fe II[19F], 76.47
5412.0	6.1	He II(2), 11.52
		Fe II(48), 14.09
		Fe II[17F], 12.64
		Fe II[16F], 12.97
5425.3	0.6	Fe II(49), 25.27
5432.7	6.2	Fe II[18F], 33.15
5476.8	6.5	Fe II[34F], 77.25
		Fe II(49), 77.67
5482.0	0.9	
5494.5	3.9	Fe II[17F], 95.82
5503.2	0.8	
5506.2	1.8	
5526.9	11.7	Fe II[17F], 27.3
		Fe II[34F], 27.61
5533.7	3.0	Fe II(55), 34.86
5545.1	1.6	Fe II[33F], 45.88
5548.8	0.7	Fe II[2F], 46.59
5553.3	0.7	Fe II[39F], 51.53
5556.9	1.7	Fe II[18F], 56.31
5580.4	3.8	Fe II[39F], 80.82
5588.8	0.5	Fe II[39F], 88.15
5612.7	1.3	Fe II[39F], 13.27
5627.3	0.5	Fe II[a2P-b2D], 27.25
5644.6	0.6	Fe II[18F], 44.0
5651.3	3.0	Fe II[39F], 50.94
5655.4	1.6	Fe II[17F], 54.85
5658.2	0.5	Fe II[33F], 59.83
5673.2	3.9	Fe II[a2G-c2G], 73.22
5690.3	0.4	Cr III[1F], 89.3
5703.9	0.3	N III[14F], 03.64
5716.1	3.1	Fe II[39F], 18.2
5720.9	0.6	Fe II[33F], 21.35
5731.6	1.0	N II(3), 30.67
5747.2	9.2	Fe II[17F], 45.7
		Fe II[34F], 46.96
5754.1	80.6	N II[3F], 54.8
5799.3	0.5	Fe II[a2P-b2D], 99.0
5810.1	0.4	Fe II[33F], 09.43
5836.1	3.1	Fe II[a2G-c2G], 35.44
5853.5	3.0	
5870.2	2.2	Fe II[a2G-a2I], 70.0
5875.1	11.6	HeI(11), 75.6
5886.5	1.7	Cr III[1], 84.9
5888.2	2.2	
5890.0	6.1	NaI(1), 89.95
5896.9	0.9	NaI(1), 5896
5901.5	2.0	Fe II[34F]. 01.26

Table 1. continued.

Wavelength	$F(\lambda)$	Identification
5956.9	9.2	Fe II, 56.5
		S III(4), 57.61
5978.6	16.1	S III(4), 78.97
5982.0	0.9	
6044.0	0.6	Fe II[a2G-a2I], 44.10
6046.4	4.6	OI(22), 46.26+46.46
6125.5	2.6	
6133.2	0.4	
6148.2	1.3	Fe II(74), 47.74
6150.0	0.7	Fe II(74), 49.24
6159.3	1.1	Fe II(161), 60.75
6174.2	0.9	N II(36), 73.40
6187.9	2.2	Fe II[44F], 88.55
6225.8	0.4	Al II(10), 26.18
6232.9	2.6	Fe I[29F], 31.27
		Al II(10), 31.78
6236.2	0.5	
6240.2	0.4	Fe II(74), 38.42
6247.4	1.4	Fe II(74), 47.562
6248.1	6.3	Fe II(z4D0-c4D), 48.92
6291.0	1.4	
6300.3	3.2	O I[1F], 00.23
6312.1	1.4	S III[3F], 12.1
6317.0	18.2	Fe II(z4D0-c4D), 17.98
6347.9	13.2	S III(2), 47.09
		N II(46)47.1
6353.5	1.1	Fe II[a2D-b2D], 53.1
6366.0	6.2	O I[1F], 63.88
		N III[8F], 65.52
6372.1	6.8	Fe II(40), 69,45
		S III(2), 71.36
6383.6	6.7	Fe II(z4D0-c4D), 83.75
6385.0	5.4	Fe II (z4D0-c4D), 85,47
6440.3	1.2	Fe II[15F], 40.40
6442.2	2.3	Fe II(c4F0-c4D), 42.97
6456.7	5.5	Fe II(74), 56.37
6473.5	0.5	Fe II[44F], 73.86
6482.4	0.9	N I(21), 81.73+82.74
		Fe II(199), 82.2
6485.1	2.2	Fe II[b4P-a2S], 85.3
		N I(21), 83.7+84.7
6491.7	3.0	N II(45), 92.0
6492.8	4.2	Fe II(z4D-c4D), 91.28
6507.2	3.8	Fe II(z4F-c4D), 06.33
6511.1	1.2	Fe II[b4F-c2D], 11.2
6517.3	9.9	Fe II(40), 16.05
6547.2	103.4	N II[1F], 48.1
6559.5	sat	Hα
6582.5	280.6	N II[1F], 83.6
6667.7	9.4	N III[2F], 66.8
6678.8	3.8	HeI(46), 78.15
6717.2	1.9	S II[2F], 16.42
6730.9	4.7	S II[2F], 30.78
6776.4	0.8	Al II(111), 75.97
6792.1	2.0	N II[7F], 94.37
6808.9	2.8	Fe II[31F], 09.21
6811.7	4.2	N III[8F], 13.73
6942.2	4.2	N II(53), 42.9
	2.4	Fe II[43F], 44.91
6964.6	1.5	Fe II[31F], 66.32
6979.2	0.5	Mn II[2F], 78.57
7001.7	3.2	Mn II[2F], 02.02
7030.1	2.6	Ni(156), 28.60
		Ni(61), 28.95
		Ni(126), 30.06
7044.9	3.5	Fe II[31F], 47.99
7052.5	1.9	Ti III[17F], 51.04
		C II(26), 52.9
7063.2	7.7	HeI(10), 65.72
7076.2	2.8	Fe II[31F], 75.26
		Fe III[9F], 78.2
7099.7	0.6	N III[13F], 02.84
7153.6	28.1	Fe II[14F], 55.14
7169.9	8.0	Fe II[14F], 71.98

the ion, the multiplet number and the rest wavelength of the transition. Frequently, more than one transition could be attributed to a single feature. In such cases we give the possible identifications. Very few conspicuous lines in the sample remain unidentified. As was mentioned before we have used the high-resolution (FEROS) data to distinguish some features that appeared blended at low resolution. This procedure allowed us to estimate the different contributions of each transition. In these cases we give in Table 1 the wavelength (for example 4414.1), the intensities (14.3 and 17.1) and the identifications (Fe II[7F] 4413.78 and Fe II[6F] 4416.27).

Balmer lines are seen in emission until H 11. The Balmer continuum is barely seen in emission. The most numerous lines however are those of the ion Fe II. More than 30 multiplets of forbidden [Fe II] transitions, as well as about 25 multiplets of permitted Fe II lines, have been identified (see Table 1). We also emphasize the remarkable intensities of [N II] lines at λ5754.8 Å [3F], 6548.1 Å and 6583.6 Å [1F]. In addition, a number of multiplets of double-ionized species are seen, in particular, forbidden transitions of [N III] and permitted transitions of S III. On the other hand, recombination lines of helium are quite weak. The [O I] [1F] multiplet is not intense too. The λ6300.2 Å transition is weak. The contribution of [O I] 6369.9 Å to the feature observed at 6366.0 Å must be small, because this transition is expected to be weaker than O I[1F]6300.2. It is likely that the major contribution is given by N III[8F]6365.5 since the transition N III[8F] at 6813.7 is also present and is quite intense. In addition, some (permitted and forbidden) lines have been attributed to other low excitation species such as Ca II, S II and Al II. Few permitted lines of neutral elements (N I, O I and Mg I) are also present. Hα is saturated in the low resolution spectra.

Almost all features reveal a double-peak emission profile when seen in high resolution. This would suggest the existence of significant rotational components in the velocity field of the emission line-forming region. P-Cygni type profiles are not seen in any line (including Balmer

recombination transitions) in the low resolution spectra. This behavior is confirmed by the high resolution data. Figure 3 shows the region around the λ5754 Å (a) and the region around Hα and [N II] (b) taken with FEROS spectrograph. The feature at 5747 Å is the sum of the transitions of Fe II at 5745.7 Å and 5746.96 Å.

2.3. Extinction

We determined the extinction parameter in the same way as Pagel (1969). We first measured the observed line fluxes of some forbidden lines (those with excitation potential between 2.5 and 3.2 eV) and between 4100 Å and 5500 Å. We then plot log I (defined below) in the ordinates against the reciprocal wavelength ($1/\lambda$ (μm)) in the abscissa. In the ordinate, log I is the difference between the logarithm of the observed flux and the logarithm of the emitted flux by the source in the same wavelength range and is defined by the relation

$$\log I = \log(F_{\rm obs}(\lambda)) - (\log(5000/\lambda) + \log(gA) - 0.56\,\chi + 2.0) \quad (1)$$

where $F_{\rm obs}(\lambda)$ is the observed line flux in units of Hβ = 100, gA, is the statistical weight multiplied by the transition probabilities and χ is excitation potential of the upper level of the transition. The factor 2.0 accounts for the log $F(\mathrm{H}\beta) = 100$.

The last column of Table 2 gives log I as defined in the text. Figure 4 shows log I plotted against the reciprocal wavelength. The value of $E(B-V)$ is obtained multiplying the difference of the values of the ordinates corresponding to the B and V-band by -2.5. The color excess $E(B-V)$ which results from this procedure is 0.93 ± 0.45.

3. Physical conditions

The excitation temperature was determined following Viotti (1969) who assumes that the forbidden lines originate in an optically thin homogeneous envelope. Since in the spectra of SS73 11 there are several emission lines of forbidden single ionized iron it is possible to derive the excitation temperature in the emitting region. Table 2 also gives the multiplet (Col. 1), the wavelength (Col. 2), the parameter β (Col. 3) defined as $\beta = \log(F_{\rm c}(\lambda)\lambda\ (\text{Å})/gA)$ and the excitation potential of the forbidden lines used in this calculation (Col. 4). In the above expression $F_{\rm c}(\lambda)$ is the line intensity in units of Hβ = 100 corrected for reddening and λ is given in Angstroms. Figure 5 shows the fit that results from the procedure outlined above. The obtained temperature based on this method is $T_{\rm exc} = 9000 \pm 2000$ K.

Table 1 reveals that the [S II] 6717/6731 ratio is approching its high density limit. With this in mind we set a lower limit for the electron density for the emitting region of SS73 11 for $N_{\rm e} \geq 10^5$ cm^{-3}. The electron density also has been estimated from the [N II] lines. The forbidden emission lines at 5754 Å, 6548 Å and

Table 2. Multiplets, wavelengths, parameter β (defined in the text), excitation potential (χ) and log I (also defined in the text) of some selected non-blended emission lines used for reddening determination and excitation temperature determination.

Multiplet	Wavelength	β	χ (eV)	log I
4F	4639.68	4.45	2.77	0.25
	4728.07	4.23	2.69	0.20
	4798.63	4.56	2.69	0.33
	4889.63	4.47	2.57	0.22
	5006.52	5.09	2.57	0.86
6F	4382.75	4.62	2.82	0.40
	4432.45	4.48	2.83	0.26
	4457.95	4.35	2.82	0.13
	4528.39	4.49	2.83	0.30
7F	4287.40	4.41	2.88	0.18
	4413.78	4.70	2.88	0.18
	4452.11	4.64	2.88	0.30
	4474.91	4.64	2.88	0.45
17F	5495.82	4.45	2.63	0.35
	5654.85	4.53	2.53	0.42
18F	5107.96	4.46	2.77	0.37
	5268.88	4.55	2.69	0.44
	5273.38	4.77	2.57	0.60
	5347.67	4.34	2.69	0.25
	5433.15	4.59	2.67	0.50
	5556.31	4.71	2.57	0.60
	5644.00	5.19	2.57	1.09
19F	5072.40	4.64	2.66	0.47
	5220.06	4.40	2.66	0.28
	5261.61	4.42	2.65	0.30
	5333.65	4.37	2.66	0.26
	5376.47	4.48	2.68	0.40
20F	4874.49	4.46	2.83	0.36
	4905.35	4.42	2.82	0.32
	4947.38	4.21	2.79	0.09
	4950.74	4.30	2.84	0.21
	4973.39	4.53	2.83	0.45
	5005.52	4.67	2.82	0.58
	5020.24	4.53	2.84	0.45
	5043.53	4.58	2.83	0.51
21F	4243.98	3.95	3.14	—
	4276.83	3.97	3.19	—
	4305.90	4.07	3.22	—
	4319.62	4.04	3.21	—
	4372.43	4.08	3.21	—
31F	6089.21	4.52	2.79	0.75
	6966.32	4.61	2.84	0.90
35F	5163.94	4.20	3.37	—
	5283.10	3.94	3.37	—
39F	5551.53	3.43	3.89	—
	5588.15	3.83	3.87	—
a2D-b2D	6553.10	3.54	4.50	—
a2G-a2I	5870.00	3.61	4.10	—
	6044.10	3.20	4.10	—
a2G-b2D	4898.61	3.59	4.50	—
	5028.20	3.95	4.50	—
	5060.08	3.68	4.50	—
a2G-c2G	5673.22	3.70	4.10	—
	5835.44	3.64	4.10	—
a2P-b2D	5627.25	3.52	4.70	—
	5799.00	3.76	4.70	—
a2P-c2D	5048.18	3.59	4.70	—

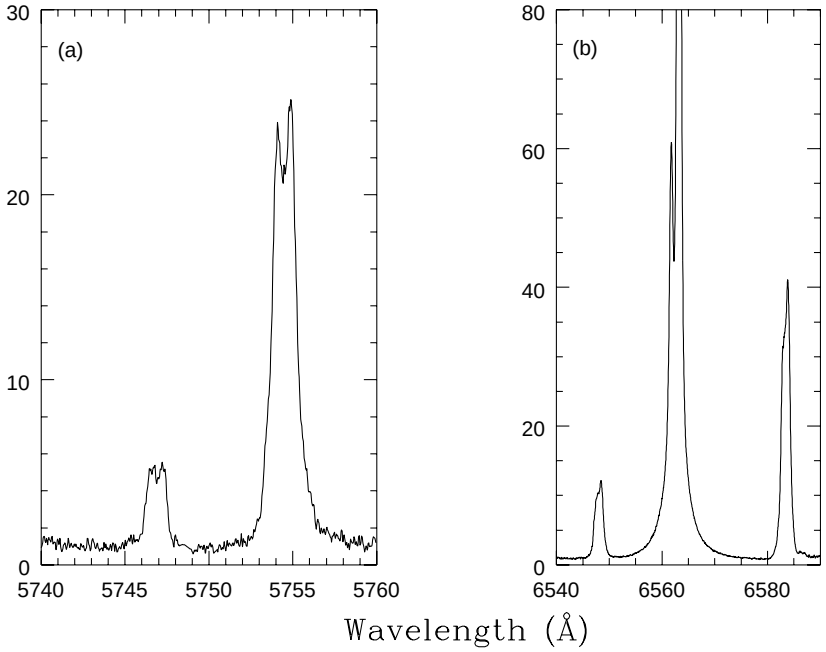

Fig. 3. High resolution spectra obtained with FEROS spectrograph in the regions around the forbidden nitrogen line at 5754 Å **a)** and around Hα **b)**.

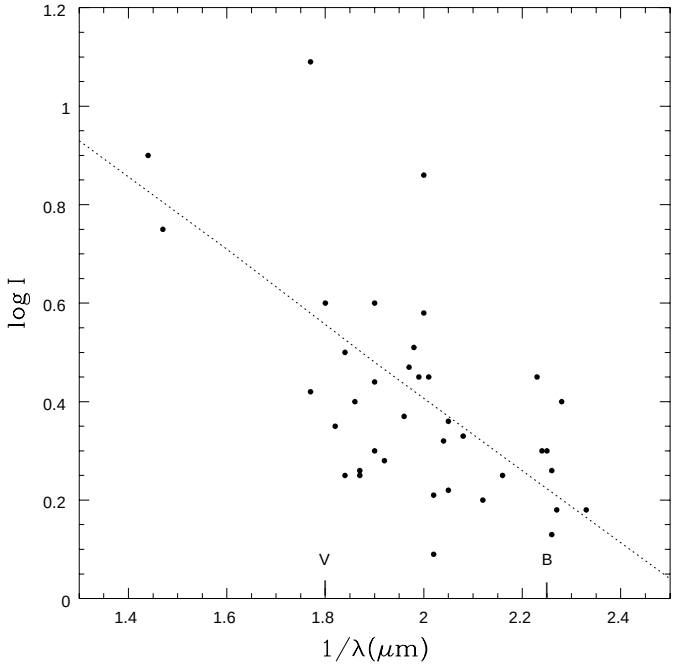

Fig. 4. log I, defined in the text, plotted against the reciprocal wavelength.

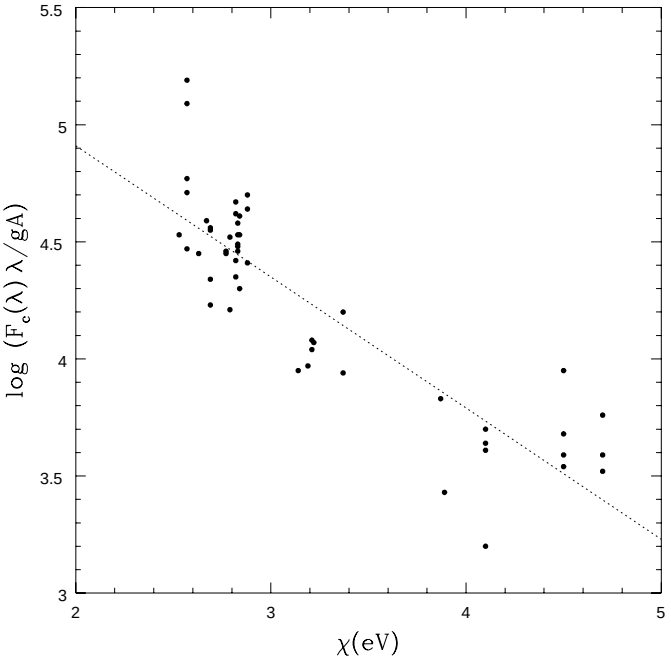

Fig. 5. Excitation temperature of SS73 11. In the ordinates we plot the parameter β, defined in the text, against the excitation potential χ. The slopes gives $T_{\rm exc} = 9000$ K.

6584 Å are present in the spectra. The dereddened ratio $(I(6548) + I(6584))/I(5754)$ of 3.2 also suggests that the emission originates in a high-density gas. Adopting $T_{\rm e} \approx T_{\rm exc}$ derived above, this ratio implies a density of $N_{\rm e} \approx 10^6$ cm^{-3}. This value is consistent with the limit estimated above.

Since the spectrum of SS73 11 presents many permitted and forbidden lines of Fe II it would be useful to apply the self-absorption curve (SAC) analysis (Friedjung & Muratorio 1987) to derive physical parameters of the emitting region. For this purpose, we select multiplets with several permitted non-blended lines, in which the intensities are correlated with the transition probabilities, within each multiplet.

Selected multiplets were grouped by similar upper and lower potentials, thereby obtaining two groups: 1) with multiplets 27, 29, 37 and 38, which serve as reference;

and 2) with multiplets 48 and 49. Each component was plotted in a graph X versus Y where X is $\log gf\lambda$ and Y is $\log F_{\rm ul}\,\lambda^3/gf$. Y is the normalized flux, $F_{\rm ul}$ denotes the extinction-corrected line intensity, λ is the wavelength and gf the oscillator strength of the transition. The components of group 2 were shifted by ΔX and ΔY to obtain the best overlap of the reference group. The ensemble of all the points can be represented by a negative slope straight line, which corresponds to an optically thick case, as shown in Fig. 6. Our data do not allow us to see the bending of the SAC curve, in the upper-left side, but the points representing the non-blended forbidden lines give a constraint to the location of the region where the thin case is attained. The point where the straight line bends to the horizontal thin case branch has $X_0 <\approx -11 \pm 0.5$ and $Y_0 <\approx -18.5 \pm 0.5$, just below the cloud of points corresponding to the forbidden lines.

Assuming as a first approximation that the logarithm of the level population is a linear function of the excitation potential and taking into account that $\Delta Y = 0.5$, we obtained an upper level excitation temperature $T_{\rm u} = 5040/\Delta Y \approx 10\,000$ K, similar to the one obtained above.

X_0 provides the value of the Fe II column density of the ground term divided by the characteristic line broadening velocity v_0, which we assume to be the thermal one. We found: $\log N_0/g_0 \approx 18$ and from that value, if all the iron is in the form of Fe II and the iron abundance is the cosmic one, the hydrogen column density is of the order of 10^{25} cm^{-2}.

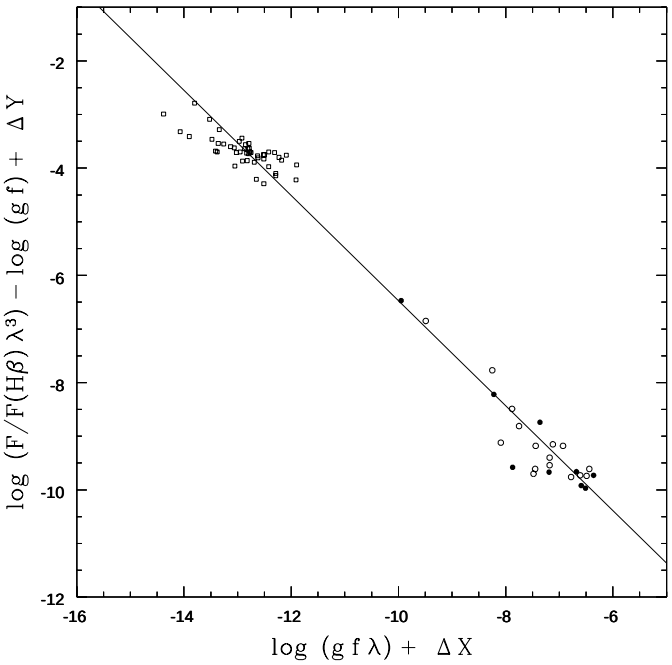

Fig. 6. Empirical Self-Absorption Curve of SS73 11 derived from Fe II multiplet overlapping. Filled circles correspond to permitted transitions of Group 1 (multiplets 27, 29, 37 and 38), open circles correspond to permitted transitions of Group 2 (multiplets 48 and 49) and open squares points to forbidden transitions. The x-axis denotes $\log(gf\lambda) + \Delta X$, the log of the optical thickness. The y-axis gives the log of the normalized flux which is equal to $\log\,(F_{\rm ul}\,\lambda^3/gf) + \Delta Y$.

4. The nature of SS73 11

The most remarkable aspect of SS73 11 is its similarity to the spectrum of the well known LBV η Car. Figures 7a and 7b show the two spectra obtained at the same resolution of 4.6 Å, in the range 3900 Å –7200 Å. The solid line is the spectrum of SS73 11 and the dotted-short dashed line is the spectrum of η Car. In spite of the similarity, small differences may be seen. For instance, [N III] and S III are clearly present in the study object but they are absent (or very weak) in η Car. At the same time SS73 11 exhibits several characteristics of the objects that display the "B[e]-phenomenon" (Lamers et al. 1998, hereafter L98). In order to better understand the nature of the studied object and also try to group SS73 11 in some known category among peculiar emission stars, we will follow the improved classification of L98. We are going to compare some of the observed spectral characteristics with those already seen in some stars displaying the "B[e] phenomenon".

The major impediment to addressing the true nature of SS73 11 is the absence of any estimate of its distance, which implies that its luminosity is also unknown. In this case, this object could be in principle categorized in any of the following groups: supergiant B[e], pre-main sequence B[e] ("HAeB[e] star") or compact planetary nebulae. On the other hand SS73 11 is definitively not a symbiotic star due to absence of any TiO absorption bands or other F-, G- or K-type features in the visual spectrum. Moreover there is no evidence of forbidden emission lines of higher ionization such as [O III], [Ne III] and [Fe VIII] and also the recombination helium line of He II, which are typical features in symbiotic spectra. SS73 11 can also not be a "HAeB[e]-star". Although several Fe II-emission lines are seen in the spectrum of V 380 Ori (L98), we did not detect an inverse P-Cygni profile in our spectrum. Besides, SS73 11 is not associated with star-forming region.

In addition to the numerous permitted and forbidden emission lines of ionized iron, a point that deserves to be emphasized is the intensity of the [N II]5754 Å which is 80% of Hβ (see Table 1). Zickgraf (1989) points out the strength of [N II] and [O I] lines as one of the spectroscopic differences in order to distinguish between supergiants B[e] and LBV in the quiescence phase. The former is stronger in LBV objects while the latter is stronger in supergiant B[e] stars. He also points that these spectroscopic characteristics could be either an effect of different excitation in the circunstellar matter or in the chemical composition in the envelope. Based on that, SS73 11 is not a B[e] supergiant, since the forbidden nitrogen line is stronger than the forbidden oxygen neutral line. Another criterion to reject SS73 11 as a supergiant B[e] is the absence of P-Cygni profiles and also the absence of absorption lines. Indeed we did not detect any of the absorptions seen by Wolf & Stahl (1985) in the spectrum of MWC 300.

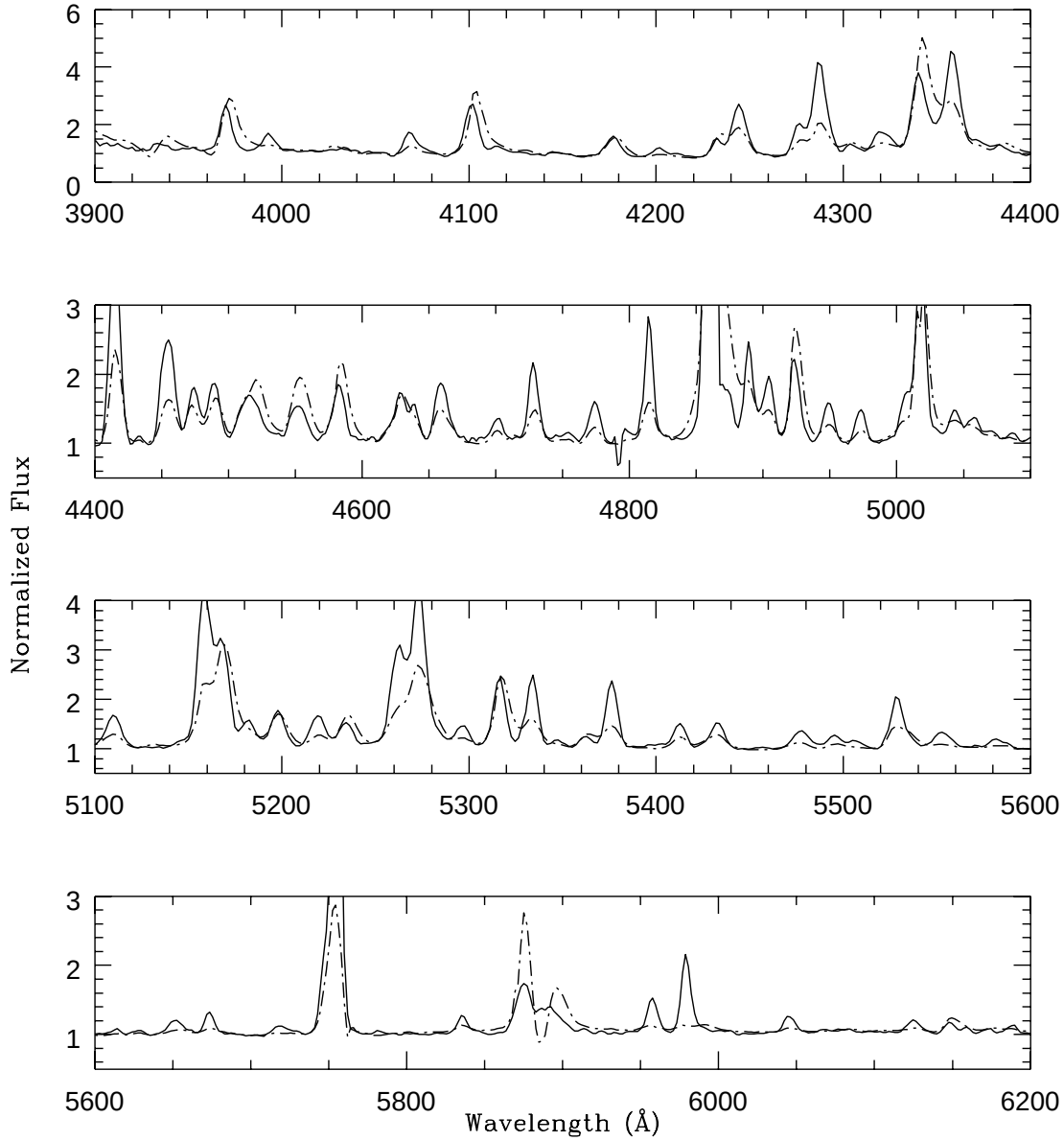

Fig. 7. a) Normalized spectra of SS73 11 and η Car. Solid line: SS73 11; Dashed-dotted line: η Car.

We have also compared our data with some compact planetary nebulae ("cPNB[e]-stars") according to the list given in Table 3 of L98. The group listed in that table have several stars whose spectra differ from each other. As an example, Hb 12, M 1-26 and Mz 3 are planetary nebulae with spectra, respectively, WN7, Of and O9.5/B0 (Acker et al. 1992). The nature of V 704 Cen is still uncertain; it might be symbiotic (Pereira et al. 1998). Hen 2-139 is a symbiotic star (Allen 1984).

The spectra of SS73 11 closely resemble those of a proto-planetary nebulae, Hen 401 (García-Lario et al. 1999), and a proto-planetary candidate, Hen 1191 (Le Bertre et al. 1989). Again the main spectroscopic difference is the strength of the [N II] line, which is much stronger in SS73 11 than in the other two objects. Moreover, [N III] is not present in Hen 1191. On the other hand, the [O I] line is strong in these two stars and weak in ours.

There are not many objects that have spectra similar to η Car. Swings & Allen (1973) realized that the spectral characteristics in the visual of MWC 645 and MWC 819 looked very similar to η Car. MWC 645 was also investigated by Jaschek et al. (1996). In fact, comparing the blue spectra of MWC 645, there are several emission lines that are also present in η Car as well as in SS73 11. Swings & Allen (1973), however, pointed that [N II]5754 Å is absent in the spectrum of MWC 645 while [O I] is strong. In MWC 819, they also remarked the presence of a very

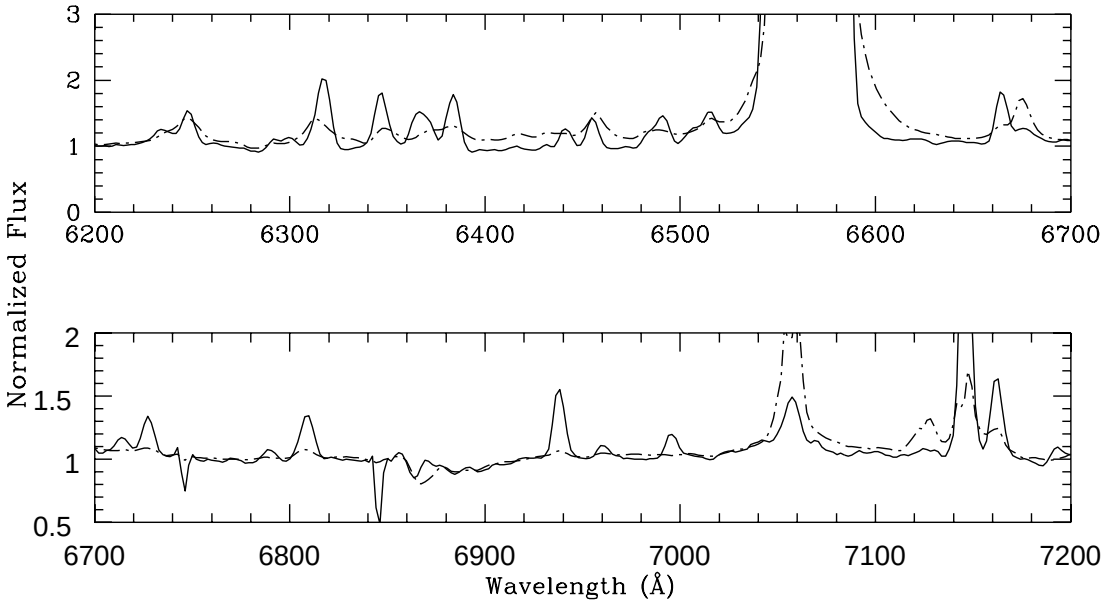

Fig. 7. b) Same as Fig. 7a.

strong line at 5754 Å . However, due to the absence of the other nitrogen lines at 6548 Å and 6584 Å, a high density effect would prevent the appearing of these two lines. If the strong line at λ5754 Å is [Fe II]λ5754.8 Å (and not [N II]5754 Å) it thus makes SS73 11 unique in itself. It is interesting to mention that SS73 11 had already been grouped by Allen & Swings (1976) together with other peculiar emission objects, among them η Car and MWC 819.

Inspecting the infrared excess as given by the IRAS flux ratio for the objects mentioned above through the Fig. 1 of Pottasch et al. (1988), only Hen 401 distinguishes itself in having similar flux ratios to planetary nebulae. The other objects, Hen 1191, MWC 819 and SS73 11 have flux ratios which place them in a region slighty above the region occupied by the OH/IR-stars. Only MWC 645 is well inside in the region of OH/IR-stars. It is worth mentioning that the presence of oxygen lines in the spectra of Hen 401, Hen 1191 and MWC 645 can be reconciled with their positions in the IRAS flux ratio diagram. This point was also stressed by Le Bertre et al. (1989) in a discussion of Hen 1191. It remains to be understood why SS73 11, having the same position in such a diagram has a very weak oxygen line.

From what was said above, the evolutionary status of SS73 11 remains unclear. This object has a spectrum which looks very similar to the spectrum of a LBV object, η Car. Several emission lines of single ionized iron that are present in SS73 11 are also present in the spectra of some proto-planetary nebulae, such as Hen 401 and Hen 1191. As was also mentioned before, the main spectroscopic difference is the strength of [N II]5754 Å in SS73 11. Although the infrared characteristics may look similar, the optical spectra can be different. On the other hand, if SS73 11 is indeed a post-AGB object, the composition of its envelope is different from some already studied, like Hen 401 and Hen 1191.

5. Summary and conclusions

We have analyzed the low- and high-resolution optical spectra of the peculiar emission-line object SS73 11. From a set of several forbidden and permitted emission lines of single ionized iron, we derived some physical conditions in the envelope, such as excitation temperature, electron temperature and density. The SAC method was used to investigate the physics of the single ionized iron region. Finally we discussed the nature of the studied object comparing it with several other peculiar emission-line objects already analyzed in the literature, which display the "B[e]-phenomenon".

The similarity between SS73 11 and η Car spectra is remarkable. However, it should be stressed that its spectrum also looks similar to those of Hen 401 and Hen 1191, two proto-planetary nebulae candidates. On the other hand, it is certain that SS73 11 is not a B[e] supergiant, a symbiotic star or a Herbig AeB[e] star.

Acknowledgements. We thank the referee, Dr. Silvia Torres-Peimbert, for valuable remarks and comments.

References

Acker, A., Chopinet, M., Pottasch, S., & Stenholm, B. 1987, A&AS, 71, 163
Acker, A., Ochsenbein, F., Stenholm, B., et al. 1992, Strasbourg-ESO Catalogue of Planetary Nebulae
Allen, D. A. 1984, PASA, 5, 369
Allen, D. A., & Glass, I. S. 1974, MNRAS, 167, 331
Allen, D. A., & Glass, I. S. 1975, MNRAS, 170, 579

Allen, D. A., & Swings, J. P. 1976, A&A, 47, 293
Friedjung, M., & Muratorio, G. 1987, A&A, 85, 233
García-Lario, P., Riera, A., & Manchado, A. 1999, ApJ, 526, 854
Hamuy, M., Suntzeff, N. B., Heathcote, S. R., et al. 1994, PASP, 106, 566
Henize, K. 1967, ApJS, 14, 125
Kaufer, A., Stahl, S., Tubbesing, S., et al. 1999, The Messanger, 95, 8
Jaschek, M., Andrillat, Y., & Jaschek, C. 1996, A&AS, 120, 99
Lamers, H. J. G. L. M., Zickgraf, F. J., de Winter, D., Houziaux, L., & Zorec, J. 1998, A&A, 240, 117 (L98)
Le Bertre, T., Epchtein, N., Gouiffes, C., Heydari-Malayeri, M., & Perrier, C. 1989, A&A, 225, 417
Moore, C. E. 1945, A Multiplet Table of Astrophysical Interest, Part I – Table of Multiplets (Revised Ed., Princeton, New Jersey: Princeton University Observatory)
Oke, J. B. 1974, ApJS, 27, 21
Pagel, B. E. J. 1969, Nature, 221, 325
Pereira, C. B., Landaberry, S. J. C., & Conceição, F. 1998, AJ, 116, 1971
Pereira, C. B., Schiavon, R. P., de Araújo, F. X., & Landaberry, S. J. C. 2001, AJ, 121, 1071
Pottasch, S. R., Bignell, C., Olling, R., & Zilstra, A. A. 1988, A&A, 205, 248
Sanduleak, N., & Stephenson, C. B. 1973, ApJ, 185, 899
Stenholm, B., & Acker, A. 1987, A&AS, 68, 51
Swings, J. P., & Allen, D. A. 1973, Astrophys. Lett., 14, 65
Thackeray, A. D. 1967, MNRAS, 135, 51
van Winckel, H., Schwarz, H. E., Duerbeck, H. W., & Fuhrmann, B. 1994, A&A, 285, 241
Velghe, A. G. 1957, ApJ, 126, 302
Viotti, R. 1969, Astrophys. Spa. Sci., 5, 323
Webster, L. B. 1966, PASP, 78, 136
Westerlund, B. E., & Henize, K. 1967, ApJS, 14, 154
Wolf, B., & Stahl, O. 1985, A&A, 148, 412
Zickgraf, F. J. 1989, in Angular Momentum and Mass Loss for Hot Stars, ed. R. A. Wilson, & R. Stalio (Kluwer Academic Publishers), 245